Tunneling decay in a magnetic field

T. Sharpee,[1] M. I. Dykman,[1,*] and P. M. Platzman[2]
[1]*Department of Physics and Astronomy, Michigan State University, East Lansing, Michigan 48824*
[2]*Bell Laboratories, Lucent Technologies, Murray Hill, New Jersey 07974*
(Received 26 June 2001; published 1 March 2002)

We provide a semiclassical theory of tunneling decay in a magnetic field and a three-dimensional potential of a general form. Because of broken time-reversal symmetry, the standard WKB technique has to be modified. The decay rate is found from the analysis of the Hamilton trajectories of the particle in complex phase space and time. In a magnetic field, the tunneling particle comes from beneath the barrier with a nonzero velocity. The exit location in the classically allowed region is obtained by matching the decaying and outgoing branches of the WKB wave function on a caustic of the set of the complex trajectories. The slope of the *logarithm* of the wave function sharply changes on the anti-Stokes surface where there occurs switching between different WKB branches. For potential wells that are parabolic near the minimum, we also provide a bounce-type formulation. The theory is applied to the models that are relevant to tunneling from correlated two-dimensional electron systems in a magnetic field parallel to the electron layer.

DOI: 10.1103/PhysRevA.65.032122 PACS number(s): 03.65.Sq, 03.65.Xp, 73.40.Gk, 73.21.−b

I. INTRODUCTION

Magnetic field can very strongly change the tunneling rate of charged particles. This change, in turn, strongly depends on properties of the system, as in the well-known effect of giant hopping magnetoresistance in solids [1]. Therefore tunneling in a magnetic field has been broadly used as a sensitive and revealing probe of electron systems in solids, including quantum Hall systems [2–5], two-layer heterostructures away from the quantum Hall region [6–9], and correlated electron layers on the surface of liquid helium [10,11].

Correlated two-dimensional (2D) electron systems are currently attracting much interest [12]. The possibility to obtain information about electron correlations and dynamics through tunneling in a magnetic field is one of the motivations of the present work. Another important motivation comes from the fact that tunneling in a magnetic field is an interesting theoretical problem, even in the single-particle formulation. Existing results, although often highly nontrivial, are limited to the cases where the potential has either a special form [13–16] (e.g., linear [13] or parabolic [15]), or a part of the potential or the magnetic field is in some sense weak [17–23].

The problem of tunneling has two parts. One is to find the tail of the wave function of the localized intrawell state under the potential barrier $U(\mathbf{r})$ and behind it, and the other is to find the escape probability W. In a magnetic field, W differs exponentially from the probability to reach the boundary of the classically allowed range $U(\mathbf{r})=E$, where E is the energy of the particle. This is because, as it tunnels, the particle is accelerated by the Lorentz force, and it comes out from the barrier with a nonzero velocity $\mathbf{v}$. The standard argument that the exit point is the turning point $\mathbf{v}=\mathbf{0}$ relies on time-reversal symmetry (see below) and does not apply in the presence of a magnetic field.

A simple potential $U(\mathbf{r})$ and the wave function $\psi(\mathbf{r})$ of the metastable state in this potential are sketched in Figs. 1 and 2. The wave function decays away from the potential well. At some point $\mathbf{r}$, on the background of the decaying tail there emerges a propagating small-amplitude wave packet, which corresponds to the escaped particle. As a result, in a part of the classically allowed region, $U(\mathbf{r})<E$, the function $\psi(\mathbf{r})$ is determined by this wave packet, whereas in the other part of this region ψ is determined by a different branch of the tail of the localized state. The boundary between these areas has a width $\propto\hbar$, and the slope of the wave function sharply changes on this boundary.

An important part of the WKB formulation of the tunneling-escape problem in a magnetic field was found in Ref. [13b] in the analysis of decay for a special model of an

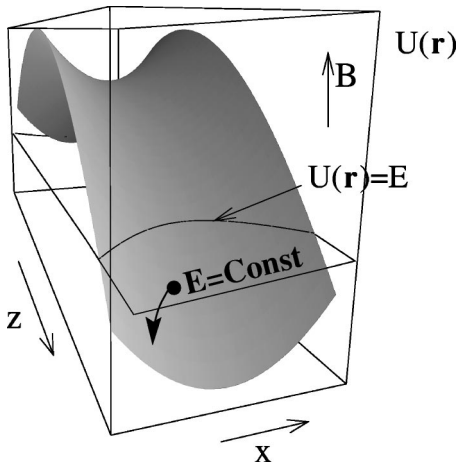

FIG. 1. Tunneling in a two-dimensional potential $U(x,z)$ transverse to a magnetic field B pointing in the y direction. Initially the particle is localized in a metastable state behind the barrier (on the small-z side) with energy E. In contrast to the case $B=0$, the particle emerges from under the barrier with a nonzero velocity, and therefore the exit point is located away from the line $U(\mathbf{r})=E$.

*Author to whom correspondence should be addressed. Email address: dykman@pa.msu.edu

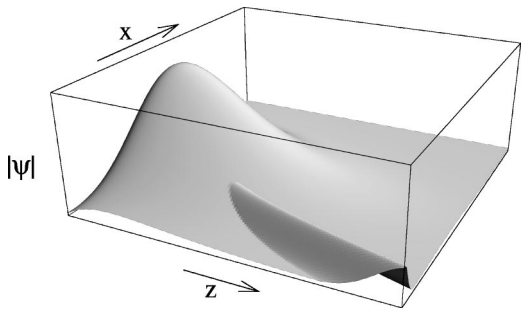

FIG. 2. The absolute value of the tunneling wave function (schematically). The maximum is located inside the potential well, i.e., behind the barrier in Fig. 1. A Gaussian wave packet of slowly varying height describes the escaped particle.

atomic system [see Eq. (9) below]. In a general case, both the tail of a metastable state and the outgoing wave packet can be found using the approach described below and briefly outlined in our paper [24].

In the WKB approximation the wave function is sought in the form

$$\psi(\mathbf{r}) = D(\mathbf{r})\exp[iS(\mathbf{r})] \quad (\hbar = 1). \tag{1}$$

Here, $S(\mathbf{r})$ is the classical action and D is the prefactor. In the classically allowed range, Eq. (1) describes a wave propagating with a real momentum $\mathbf{p} = \boldsymbol{\nabla} S$. In the classically forbidden range the wave function decays. For the ground intrawell state, this decay is not accompanied by oscillations in the absence of a magnetic field. Then the action $S(\mathbf{r})$ is purely imaginary under the barrier and $|\boldsymbol{\nabla} S|$ is the decrement of the wave function.

Both behind and inside the barrier, the action can be obtained from the Hamilton equations of motion

$$\dot{S} = \mathbf{p}\cdot\dot{\mathbf{r}}, \quad \dot{\mathbf{r}} = \partial H/\partial \mathbf{p}, \quad \dot{\mathbf{p}} = -\partial H/\partial \mathbf{r}, \tag{2}$$

where H is the Hamiltonian of the tunneling electron,

$$H = \frac{1}{2m}\left[\mathbf{p} + \frac{e}{c}\mathbf{A}(\mathbf{r})\right]^2 + U(\mathbf{r}), \tag{3}$$

[$\mathbf{A}(\mathbf{r})$ is the vector potential of the magnetic field].

In the standard approach to tunneling decay, which applies for $B = 0$ [14,25–28], the purely imaginary action S under the barrier is calculated by changing to imaginary time and momentum in Eqs. (2), but keeping coordinates real,

$$t \to -it, \quad \mathbf{p} \to i\mathbf{p}, \quad \mathbf{r} \to \mathbf{r}, \quad U(\mathbf{r}) \to -U(\mathbf{r}). \tag{4}$$

Equations (2) then take the form of equations of classical motion in an inverted potential $-U(\mathbf{r})$, with energy $-E \geqslant -U(\mathbf{r})$. The imaginary-time trajectory goes from the turning point on the boundary of the potential well to the turning point on the boundary of the classically allowed region, where it matches the appropriate classical trajectory of the escaped particle behind the barrier, with real $\mathbf{r}, \mathbf{p}, t$. The velocities on the trajectories can coincide at the matching point only if $\mathbf{v} = \mathbf{0}$.

In the presence of a magnetic field, because of broken time-reversal symmetry, the replacement (4) may not be performed. It would lead to a complex Hamiltonian, which makes no sense and indicates that a more general approach is required. The action $S(\mathbf{r})$ is complex under the barrier for real $\mathbf{r}$. This complexity plays an important role in the instanton formulation of the problem of tunneling decay in a magnetic field discussed below. Complex action arises also in other problems, such as tunneling splitting in an ultrastrong magnetic field [18], barrier penetration for oblique incidence [29], and scattering by a complex potential (as in the case of an absorbing medium) [30]. The method discussed below can be applied to many of these problems.

In this paper we consider a single-particle tunneling decay into extended states in a three-dimensional potential of a general form for arbitrary magnetic fields. We illustrate the approach using a toy model of a correlated 2D electron system. We show that the exponent $S(\mathbf{r})$ and the escape rate in a magnetic field can be found from dynamical equations (2) by analytically continuing these equations to complex phase space and time. The initial conditions for the trajectories are determined by the analytical continuation of the usually known intrawell wave function. The resulting set of complex trajectories has singularities, caustics, which are envelopes of the trajectories. The complex action $S(\mathbf{r})$ is branching on the caustics, and tails of the decaying and propagating waves are matched there. Careful analysis allows us to find the complete semiclassical wave function and reveal the singular features of $\psi(\mathbf{r})$ related to the branching of S.

In Sec. II and Appendix A we provide a simple but nontrivial model, which, in particular, captures basic physics of tunneling from correlated 2D electron layers. In Sec. III we consider the tunneling exponent and formulate the boundary-value problem for tunneling trajectories in a magnetic field in complex phase space. In Sec. IV we discuss matching of different semiclassical solutions across the caustic of the set of the tunneling trajectories. We show that a switching surface (one of the anti-Stokes manifolds) starts at the caustic. The wave function has an observable singular feature at this surface, which is a sharp change of the slope of $\ln|\psi(\mathbf{r})|$. In Sec. V we provide explicit results for two simple exactly solvable models of physical interest, which also illustrate general features of tunneling in a magnetic field. In Sec. VI we discuss the path-integral formulation of the problem of tunneling decay in a magnetic field. Section VII contains concluding remarks.

II. A MODEL OF THE TUNNELING BARRIER

A physical system that allows one to reveal and investigate specific features of 3D tunneling in a magnetic field and where the effect of a magnetic field on tunneling has been investigated experimentally is a correlated 2D electron system (2DES). We will use it in order to formulate a tractable model and illustrate our general results. In a 2D system, elec-

trons are localized in the z direction in a metastable potential well $U_0(z)$. The intrawell electron motion is quantized in the z direction, and electrons can tunnel from the well into extended states. Many 2D systems of current interest are strongly correlated. Electrons are far away from each other, exchange is weak, and there is at least short-range order in the (x,y) plane. The tunneling electron can be then identified and ''labeled.'' Its tunneling motion is accompanied by motion of other electrons. The many-electron dynamics of a correlated system can be described in terms of in-plane electron vibrations, and the corresponding Hamiltonian is given in Appendix A assuming that the electrons form a Wigner crystal. Here we will make a further simplification and think of an electron as tunneling in a static potential created by all other electrons. As we showed earlier, this is a good approximation for the tunneling problem [11].

The static potential from surrounding electrons can be assumed to be parabolic with respect to the in-plane coordinates x,y. If the characteristic width L of the tunneling barrier is less than the interelectron distance, the overall potential is a sum of the parabolic in-plane part and $U_0(z)$,

$$U(\mathbf{r})=\frac{m\omega_0^2}{2}(x^2+y^2)+U_0(z). \tag{5}$$

The form of $U_0(z)$ depends on the system. Inside the well U_0 is often singular, as in the case of electrons on helium, where U_0 includes the image potential. Important simple forms of the potential barrier are a square barrier, as in the case of unbiased semiconductor heterostructures, or a nearly linear one, as in the presence of strong enough bias voltage, with

$$U_0(z)=\frac{\gamma^2}{2m}\left(1-\frac{z}{L}\right) \tag{6}$$

inside the barrier. In what follows, we will set the energy of the out-of-plane motion $E=0$. Then γ in Eq. (6) characterizes the decay of the wave function close to the well (the reciprocal intrawell localization length) and L is the barrier width for $B=0$. The potential (6) describes, in particular, the barrier for a correlated 2DES on a helium surface. For this system, an unexpected dependence of the tunneling rate on B and electron density was observed [10] and recently addressed theoretically [11,24].

III. THE TUNNELING EXPONENT

For a smooth tunneling barrier $U(\mathbf{r})$, the underbarrier wave function $\psi(\mathbf{r})$ [Eq. (1)] can be obtained from the tunneling trajectories (2). The initial conditions for these trajectories are determined by the tail of the intrawell wave function close to the well. To find them, we can take a surface Σ close to the well, but under the barrier, where $U(\mathbf{r})$ is smooth (even if it is singular inside the well). The wave function $\psi(\mathbf{r})$ on Σ is presumably known from the solution of the Schrödinger equation inside the well and is semiclassical. Only the exponent of this wave function is needed to find the initial conditions for Eqs. (2). They take the form

$$\mathbf{r}(0)=\mathbf{r}|_\Sigma, \quad \mathbf{p}(0)=-i[\boldsymbol{\nabla}\ln\psi(\mathbf{r})]_\Sigma, \tag{7}$$

with the action $S(0)=-i[\ln\psi(\mathbf{r})]_\Sigma$. Only the lowest-order terms in $\hbar$ should be kept in the expressions for $\mathbf{p}(0),S(0)$. The final result should be independent of the choice of Σ.

The trajectories (2) with the initial conditions (7) form a *two-parameter* set in the case of 3D tunneling. The two parameters are the initial coordinates on the surface Σ. We can choose curvilinear coordinates (x_1,x_2,x_3) so that $x_3|_\Sigma \equiv x_3(0)=0$. The trajectories are then parametrized by $x_1(0),x_2(0)$.

To illustrate these arguments we consider the initial conditions for an electron with the potential (5), (6), which tunnels from a 2D layer. Inside the metastable potential well the electron motion separates into a quantized motion in the normal to the layer z direction and in-plane vibrations. To slightly simplify the analysis, we will neglect the effect of a magnetic field on the wave function inside the well, but not on the tail of $\psi(\mathbf{r})$ in a much broader region under the barrier, where the field effect accumulates. This is a good approximation for not too strong fields, provided the characteristic intrawell localization length is small compared to the tunneling length.

It is convenient then to choose the surface Σ as a plane $z=\text{const}$ close to the well. We set $z=x_3=0$ on Σ and choose $x_1=x$, $x_2=y$. If the electron is in the ground intrawell state with $E=0$, we obtain from Eqs. (5) and (6),

$$z(0)=0, \quad p_z(0)=i\gamma, \quad S(0)=im\omega_0[x^2(0)+y^2(0)]/2,$$

$$p_x(0)=im\omega_0 x(0), \quad p_y(0)=im\omega_0 y(0). \tag{8}$$

In the general case, to find the trajectory that arrives at a given real $\mathbf{r}$ deep under the barrier, it may be necessary to use *complex* $\mathbf{r}(0)$. The corresponding values of $\mathbf{p}(0)$ can be found by analytically continuing the intrawell wave function to complex $\mathbf{r}$. The whole trajectory will then go in complex phase space $(\mathbf{r},\mathbf{p})$ and also in complex time t. The energy of the trajectory is given by the energy of the intrawell state from which the system tunnels. It remains real.

The rate of tunneling decay is determined by $\mathrm{Im}\,S$ at the point where the particle emerges from the barrier as a semiclassical wave packet. This wave packet propagates along a *real* classical trajectory $\mathbf{r}_{\mathrm{cl}}(t)$, which is a real-time solution of the Hamilton equations (2). The underbarrier trajectory for tunneling escape should go over into the trajectory $\mathbf{r}_{\mathrm{cl}}(t)$. Therefore at some time t both the coordinate and velocity should become real,

$$\mathrm{Im}\,\mathbf{r}(t)=\mathrm{Im}\,\mathbf{p}(t)=0. \tag{9}$$

Equations (9) determine the complex starting point of the trajectory for tunneling escape $\mathbf{r}(0)$ [i.e., the complex $x_{1,2}(0)$, since $x_3(0)=0$] and also the imaginary part of the duration of motion along this trajectory $\mathrm{Im}\,t$. The real part of t remains undetermined: a change in $\mathrm{Re}\,t$ in Eq. (9) results just in a shift of the particle along the classical trajectory $\mathbf{r}_{\mathrm{cl}}(t)$, see Fig. 3. Such a shift does not change $\mathrm{Im}\,S$, since $\mathbf{p}=\boldsymbol{\nabla}S$ is real along $\mathbf{r}_{\mathrm{cl}}(t)$. We note that the number of equations (9) is equal to the number of variables $\mathrm{Re}\,x_{1,2}(0)$,

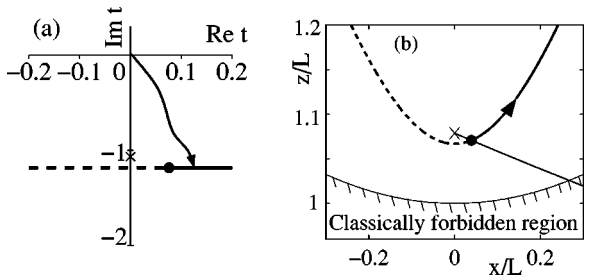

FIG. 3. (a) Complex t plane for integrating the Hamilton equations (2) in the escape problem. The line $\mathrm{Im}\, t = \mathrm{const}$ corresponds to the classical trajectory of the escaped electron, which is shown in (b). Bold solid lines in (a) and (b) indicate the range where the amplitude of the propagating wave exceeds the amplitude of the decaying underbarrier wave function. The escaped particle shows up as a semiclassical wave packet, with a nonzero velocity, at the point (full circle) where the classical trajectory intersects the switching line [thin solid line in (b)]. The crosses mark the value of t (a) and the position (b) of the caustic where it goes through real space. The specific data refer to tunneling through the potential barrier (5),(6) transverse to a magnetic field, which points in the y direction, with $\omega_0\tau_0 = 1.2$ and $\omega_c\tau_0 = 1.2$; time in (a) is in the units of $\tau_0 = 2mL/\gamma$. For the chosen parameter values, the escape trajectory hits the caustic for complex $\mathbf{r}$. The time when it happens is numerically very close to the position of the cross in (a).

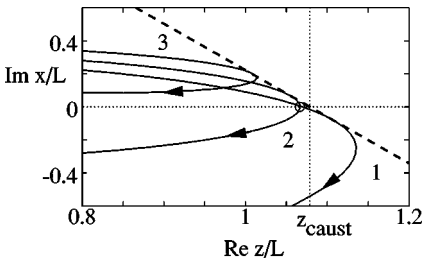

FIG. 4. The set of tunneling trajectories (solid lines) with $\mathrm{Re}\, x = \mathrm{Im}\, z = 0$ and the caustic (dashed line) for an effectively 2D tunneling problem. The data refer to the potential (5),(6) and a magnetic field along the y axis. The parameters are the same as in Fig. 3. The classical trajectory of the escaped electron is the real-time continuation of the trajectory 2 from the point $\mathrm{Im}\, x = 0$ shown by the open circle. The momentum $\mathbf{p}$ is real at this point, as explained in Sec. V A. Other trajectories do not describe escape, since on these trajectories the necessary conditions $\mathrm{Im}\, \dot{z} = \mathrm{Im}\, x = 0$ [Eq. (9)] are never satisfied. The caustic goes through real space at the point $z = z_{\mathrm{caust}}, \mathrm{Im}\, x = 0$ (the intersection of the dotted lines). The trajectory of the escaped electron does *not* go through this point.

$\mathrm{Im}\, x_{1,2}(0)$, and $\mathrm{Im}\, t$, with account taken of energy conservation. The conditions (9) were first given [13b] for a δ-shaped potential well and a linear tunneling barrier, but only the condition $\mathrm{Im}\, \mathbf{r}(t) = 0$ was explicitly used.

In the absence of a magnetic field, we can choose the surface Σ such that the momentum $\mathbf{p}|_\Sigma$ is imaginary for real $\mathbf{r}$. The equations of motion (2) can then be solved in purely imaginary time, with real $\mathbf{r}(t)$ and imaginary $\mathbf{p}(t)$, i.e., decay of the localized wave function is not accompanied by oscillations. The escape trajectory ends at the turning point $\mathbf{p} = \mathbf{0}$, even for a multidimensional system [28].

The tunneling exponent R is given by the value of $\mathrm{Im}\, S$ at any point on the trajectory $\mathbf{r}_{\mathrm{cl}}$,

$$R = 2\, \mathrm{Im} S(\mathbf{r}_{\mathrm{cl}}). \tag{10}$$

For a physically meaningful solution, $\mathrm{Im}\, S$ should have a parabolic minimum at $\mathbf{r}_{\mathrm{cl}}$ as a function of the coordinates transverse to the trajectory. The outgoing wave packet will then be Gaussian near the maximum.

From Eq. (9), even in the presence of a magnetic field the tunneling exponent can be obtained by solving the equations of motion (2) in imaginary time, with complex $\mathbf{r}$. However, such a solution does not give the wave function for real $\mathbf{r}$ between the well and the classical trajectory $\mathbf{r}_{\mathrm{cl}}$. Nor does it tell us where the particle shows up on the classical trajectory.

IV. BRANCHING OF THE ACTION AND ITS OBSERVABLE CONSEQUENCES

The complete WKB solution of the tunneling problem can be obtained and the wave function $\psi(\mathbf{r})$ can be found if one takes into account that the action S as given by Eqs. (2) is a multivalued function of $\mathbf{r}$, even though it is a single-valued function of t and $x_{1,2}(0)$. This means that several trajectories (2) with different t and $x_{1,2}(0)$ can go through one and the same point $\mathbf{r}$. However, except for the points on the switching surface (see Sec. IV D), only one of the branches of the action $S(\mathbf{r})$ contributes to the wave function $\psi(\mathbf{r})$.

A. Caustics in a magnetic field

In multidimensional systems, branching of the semiclassical action generally occurs on caustics, or envelopes of the Hamilton trajectories [31,32], see Fig. 4. Caustics are multidimensional counterparts of turning points familiar from the analysis of tunneling in 1D systems [33]. The prefactor $D(\mathbf{r})$ in the WKB wave function (1) diverges at a caustic. In the case of 1D semiclassical motion along the z axis we have $D \propto p_z^{-1/2}$, and $D \to \infty$ at turning points z_t, which are given by the condition $p_z = 0$. The action is branching at turning points, $S(z) - S(z_t) \propto (z - z_t)^{3/2}$. The behavior of S near caustics in a multidimensional system is very similar (see below), with $z - z_t$ corresponding to the distance from the caustic.

Since neighboring Hamilton's trajectories (2), (7) touch each other on a caustic, the one-to-one correspondence between the coordinates x_1, x_2, x_3 on the trajectory and the parameters t, $x_1(0)$, $x_2(0)$ breaks. Therefore the equation for a caustic has the form

$$J(\mathbf{r}) = 0, \quad J(\mathbf{r}) = \frac{\partial(x_1, x_2, x_3)}{\partial[x_1(0), x_2(0), t]}. \tag{11}$$

The Jacobian $J(\mathbf{r})$ can be related in a standard way to the prefactor $D(\mathbf{r})$, which in turn is determined by the first-order (in $\hbar$) correction to the action $-iS^{(1)}$, $D(\mathbf{r}) = \exp[S^{(1)}(\mathbf{r})]$. The equation for $S^{(1)}(\mathbf{r})$ can be obtained from the Schrödinger equation by seeking the wave function in the form $\psi = \exp(iS)$, with $S = S^{(0)} - iS^{(1)}$. This gives $2\mathbf{v}\boldsymbol{\nabla} S^{(1)} = -\boldsymbol{\nabla}\mathbf{v}$, where $m\mathbf{v} = \boldsymbol{\nabla} S^{(0)} + (e/c)\mathbf{A}$. The vector $\mathbf{v}$ gives the

velocity on the Hamilton trajectory (2). Taking into account that $\mathbf{v}\nabla S^{(1)}(\mathbf{r}) \equiv dS^{(1)}/dt$ and that $\nabla \mathbf{v} = d \ln J(\mathbf{r})/dt$, where the time derivatives are taken along the trajectory, we obtain

$$D(\mathbf{r}) = \text{const} \times [J(\mathbf{r})]^{-1/2}. \tag{12}$$

It follows from Eqs. (11), (12) that the prefactor D diverges on caustics, and the WKB approximation does not apply there [31].

There are both formal and physical distinctions between caustics for tunneling trajectories with and without a magnetic field. For $B \neq 0$, the trajectories are complex, and Eq. (11) specifies a complex surface. This surface intersects the real 3D space along a line. In contrast, for $B = 0$, because of time-reversal symmetry, tunneling trajectories lie in real configuration space. In this case Eq. (11) specifies a surface [28] rather than a line in the 3D space. This distinction leads to observable consequences.

B. Local analysis near caustics

The analysis of the wave function and branching of the action $S(\mathbf{r})$ at complex caustics in the magnetic field is similar to that for caustics in real space, including turning points in the 1D case [31]. Near a caustic, it is convenient to change to variables x', y', and z', which are locally parallel and perpendicular to the caustic surface, respectively (we set $z' = 0$ on the caustic). Since a caustic is an envelope of the Hamilton trajectories (2), the normal to the caustic component of the velocity is $v_{z'} = 0$ for $z' = 0$. However, for $B \neq 0$ the normal component of the momentum is not equal to zero, nor are the tangential components. Therefore the wave function near a point $\mathbf{r}_{\text{caust}}$ on the caustic can be sought in the form

$$\psi(\mathbf{r}_{\text{caust}} + \mathbf{r}') = e^{i\mathbf{p}_{\text{caust}} \cdot \mathbf{r}'} \phi(z'; \mathbf{r}_{\text{caust}}), \tag{13}$$

where $\mathbf{p}_{\text{caust}}$ is the momentum at the point $\mathbf{r}_{\text{caust}}$ (we note that $\mathbf{r}_{\text{caust}}$ is a 2D complex vector, $z'_{\text{caust}} \equiv 0$). We consider the case where the dependence of $\mathbf{p}_{\text{caust}}$ on the position $\mathbf{r}_{\text{caust}}$ along the caustic is smooth, and the dependence of ϕ on $\mathbf{r}_{\text{caust}}$ is much weaker than on z'. Generally, $\mathbf{p}_{\text{caust}}$ is complex even where the caustic goes through real space, $\text{Im}\mathbf{r}_{\text{caust}} = 0$. Therefore the classical trajectory of the escaped particle does not go through a caustic, in contrast to the case of zero magnetic field, cf. Fig. 4.

Because $v_{z'} = 0$ for $z' = 0$, the equation for $\phi(z'; \mathbf{r}_{\text{caust}})$, which follows from the 3D Schrödinger equation with a magnetic field, coincides with the 1D Schrödinger equation near a turning point without a magnetic field,

$$\left[-\frac{1}{2m} \frac{d^2}{dz'^2} + U'_{z'}(\mathbf{r}_{\text{caust}}) z' \right] \phi(z'; \mathbf{r}_{\text{caust}}) = 0 \tag{14}$$

(here, $U'_{z'} \equiv \partial U / \partial z'$).

The function ϕ is single valued. It is given by a linear combination of the Airy functions [33]. For comparatively large $|z'|$ (but still close to the caustic) it becomes a linear combination of the functions

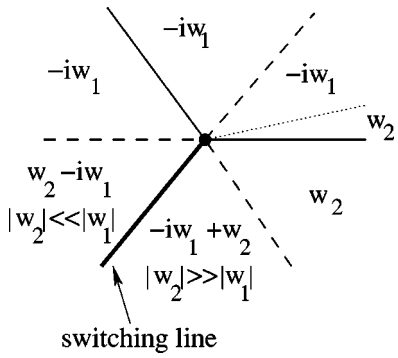

FIG. 5. The function $\phi(z')$ [Eq. (14)] for large $|z'|$ on the complex z' plane perpendicular to the caustic surface. The dashed lines, $\arg z' = (2n+1)\pi/3$, show the Stokes lines where the ratio of the functions $|w_2/w_1|$ [Eq. (15)] reaches its maximum or minimum. The anti-Stokes lines (solid lines), $\arg z' = 2n\pi/3$, are the lines where $|w_1| = |w_2|$. At these lines the ratio $|w_2/w_1|$ changes from exponentially large to exponentially small with varying $\arg z'$. The coefficients are found from the radiation boundary condition following the Stokes prescription [31]. The dotted line shows the branch cut.

$$w_{1,2} = (z')^{-1/4} \exp[\mp i \alpha z'^{3/2}], \tag{15}$$

with $\alpha \equiv \alpha(\mathbf{r}_{\text{caust}}) = (2/3)[-2mU'_{z'}]^{1/2}$. To make the functions $w_{1,2}$ uniquely defined, we have to make a cut on the complex z' plane. Our choice of the cut is shown in Fig. 5 with a dotted line.

With account taken of Eq. (13), we find that the action near the caustic is

$$S(x', y', z') \approx S(x', y', 0) + (p_{\text{caust}})_{z'} z' + \alpha z'^{3/2}, \tag{16}$$

with an appropriately chosen branch of $z'^{3/2}$. Another way to understand the nonanalyticity of S is based on the analysis of the set of the Hamilton trajectories (2). Because the caustic is an envelope of the trajectories and $v_{z'} = 0$ on the caustic, z' is quadratic in the increments $\delta x_{1,2}(0), \delta t$ of the parameters of the set. Therefore $\delta x_{1,2}(0), \delta t$ are nonanalytic in z'. Taking into account cubic terms in the expansion of S in $\delta x_{1,2}(0), \delta t$, we obtain Eq. (16). The coefficients in S can be expressed in terms of the derivatives of $S, \mathbf{r}$ as given by Eqs. (2) over $x_{1,2}(0), t$.

C. Choosing branches of the action

Equation (14) describes how the WKB solutions, which correspond to different branches of the action S, connect on the caustic. Of interest for the problem of tunneling escape is the caustic where the intrawell wave function and the outgoing wave packet for the escaped particle are connected. From Eq. (11), on this caustic there is a point through which there goes the Hamilton trajectory (2), (7) for escape, with the initial coordinates $x_{1,2}(0)$ given by the condition (9) of arriving, ultimately, at the classical outgoing trajectory $\mathbf{r}_{\text{cl}}$, cf. Fig. 4.

In general, a caustic can be thought of as a "mirror," which partly reflects the wave packet. The boundary condition to Eq. (14) for the tunneling-escape problem is the "ra-

diation condition.'' Far from the potential well the solution of the full Schrödinger equation is a semiclassical wave packet moving in real space away from the well. Respectively, the wave function far from the well has a form $\psi(\mathbf{r}) \propto \exp[iS(\mathbf{r})]$. This solution has to be continued to the complex caustic, which means that there is a range of directions in the complex z' plane not too close to the caustic ($|\alpha z'^{3/2}| \gg \hbar$) where the wave function is described by only one exponential $\exp[iS(\mathbf{r})]$. Away from this range, the wave function is a combination of two waves. This is again similar to a 1D problem, where behind the turning point z_t the wave function for real z is a propagating wave, whereas before z_t there is a wave with an exponentially decaying amplitude coming from the intrawell state, and the wave which is reflected back to this state.

To connect the tails of the wave functions near the caustic in our problem one can use the explicit solution of Eq. (14) with the radiation boundary condition, as in the 1D case [33]. An alternative way to see how the boundary condition works, which also allows us to reveal the specific feature of tunneling in a magnetic field, is to follow the transformation of the wave function ϕ for $|\alpha z'^{3/2}| \gg \hbar$ as the argument of z' varies by 2π. This analysis is based on the notion of the Stokes and anti-Stokes lines and is an extension of the Stokes-lines-based approach in the WKB approximation [31,34,35] to the case where a caustic lies in complex space. We give it here for completeness.

We count $\arg z'$ off from $-\arg \alpha^{2/3}$. Then, for the choice of the cut in Fig. 5 and with the functions $w_{1,2}$ given by Eq. (15), in the vicinity of the caustic, the Stokes lines are the rays $\arg z' = (2n+1)\pi/3$ with $n=0,1,2$. On the Stokes lines $\mathrm{Re}\, z'^{3/2} = 0$ and the ratio $|w_2/w_1|$ is extremal (maximal or minimal). The anti-Stokes lines are the rays $\arg z' = 2n\pi/3$ with $n=0,1,2$, where $|w_2/w_1| = 1$.

From the radiation boundary condition, there is a range Δ of $\arg z'$ where $\phi(z')$ is given by only one of the functions $w_{1,2}(z')$, not by a superposition of w_1 and w_2. This condition is physically meaningful provided the corresponding w_i is exponentially *small* compared to w_{3-i} in a part of the range Δ. [Otherwise the condition $\phi(z') = \mathrm{const} \times w_i$ is not a limitation, in the WKB approximation.] For concreteness, we will assume that Δ contains the range between semiaxis $\arg z' = 0$ and the cut in Fig. 5, and that in this range $\phi(z') = Cw_2(z') \propto \exp[i|\alpha|z'^{3/2}]$ is exponentially small. Here, C is a constant (it is left out in Fig. 5).

Since the function $\phi(z')$ is single valued, if we cross the cut in Fig. 5 by incrementing $\arg z'$, $\phi(z')$ becomes equal to $-iCw_1(z')$. It remains exponentially small as $\arg z'$ grows up to $2\pi/3$, including the Stokes line $\arg z' = \pi/3$. Then behind the anti-Stokes line at $\arg z' = 2\pi/3$, the function w_1 becomes exponentially big. It is important that, on the Stokes line $\arg z' = \pi$, one has to take into account the admixture to ϕ of an exponentially small term $\propto w_2(z')$. This can be seen from the explicit solution for ϕ and can be understood by noticing that when we increment $\arg z'$ by 2π, we have to recover the original asymptotic form of ϕ. This latter argument explains the coefficient at w_2 in Fig. 5.

On the anti-Stokes line $\arg z' = 4\pi/3$, the values of $|w_1|$ and $|w_2|$ become equal to each other, and $\phi(z')$ is primarily determined by w_2 for larger $\arg z'$. After $\arg z'$ crosses the Stokes line $5\pi/3$, the exponentially small term w_1 in $\phi(z')$ disappears, according to the Stokes prescription [31].

Since we chose the irradiated wave to be $\propto w_2(z')$, the asymptotic behavior of the wave function of the metastable state within the range $2\pi/3 < \arg z' < 4\pi/3$ is given by $w_1(z')$. We note that, for the radiation boundary condition, the switching between the wave functions occurs only on one of the anti-Stokes lines.

D. Switching between the branches of the wave function

Switching between the WKB wave function of the localized state and the outgoing wave packet is an important observable consequence of the analysis in the preceding section. It is due to branching of the WKB action. The switching manifold starts on the caustic and is given by the condition $\mathrm{Im}\, S_1(\mathbf{r}) = \mathrm{Im}\, S_2(\mathbf{r})$, where $S_{1,2}$ are the actions for the corresponding WKB branches. On the opposite sides of the switching manifold one of the WKB wave functions is exponentially bigger than the other.

In the presence of a magnetic field, caustics go through real space along the lines given by the condition $J(\mathbf{r}) = 0$, $\mathrm{Im}\, \mathbf{r} = 0$, with $\mathbf{r} \equiv \mathbf{r}(x_{1,2}(0), t)$ being a point on the Hamilton trajectory (2), (7). The switching manifold in real space is a surface that starts from the caustic line and goes away from it *in one direction*. Although the wave function is continuous on this surface, the derivative of its logarithm sharply changes from ∇S_1 to ∇S_2.

The exit point $\mathbf{r}$ in the configuration space where the escaped particle emerges from under the barrier is determined by the intersection of the classical escape trajectory $\mathbf{r}_{\mathrm{cl}}(t)$ and the switching surface. This point should be found from the global analysis of the WKB wave function. It does not lie on the caustic, nor is it given by the condition $\mathbf{p} = \mathbf{0}$ or $U(\mathbf{r}) = E$. In a 2D system the caustic pierces real space at a point, and the switching surface becomes a line. An example of the caustic, the switching line, and the exit point for a 2D system is shown in Fig. 3.

In the absence of a magnetic field, as we mentioned before, the caustic for tunneling trajectories is a surface rather than a line in real configuration space. The switching manifold starts at the caustic and goes into complex space. The exit point is the turning point $\mathbf{p} = \mathbf{0}$, and S has zero slope normal to the caustice surface. In contrast, in a magnetic field different action branches have different nonzero (complex) slopes normal to the switching surface. The topologies for $B = 0$ and $B \neq 0$ cases are thus very different.

V. TUNNELING FROM A CORRELATED 2D ELECTRON SYSTEM

We now apply the general approach to tunneling from a correlated 2D electron system transverse to a magnetic field and illustrate the occurrence of the singularities discussed above. We use the simple but nontrivial model of an electron system discussed in Sec. II and described by Eqs. (5),(6),

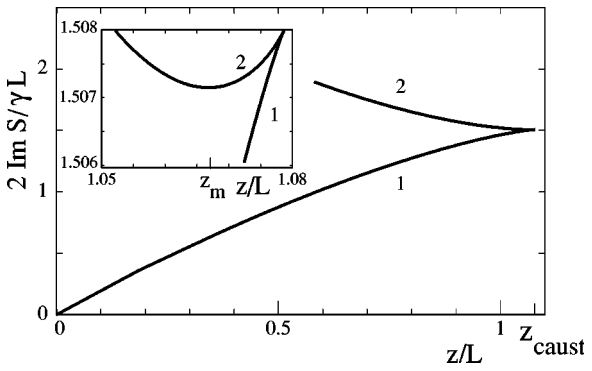

FIG. 6. Two branches of the action on the symmetry axis $x=0$ as a function of the tunneling coordinate z before the branching point (cusp) $z_{\mathrm{caust}}\approx 1.078$, for the symmetric model (5) and the same parameter values as in Fig. 3. The vicinity of the cusp is zoomed in the inset to show that the upper branch is nonmonotonic. Its extremum at z_m lies on the classical trajectory of the escaped particle shown in Fig. 3(b). However, the particle emerges from the barrier for $z>z_m$ and $x\neq 0$.

and its generalization to the case of broken in-plane symmetry. We assume that the magnetic field is parallel to the electron layer, and choose the y axes along the field **B**.

A. A model with in-plane symmetry

For an electron in the potential (5), (6), classical motion along the $\mathbf{B}\|\hat{\mathbf{y}}$ axis is decoupled from motion in the (x,z) plane. The WKB tunneling problem then becomes two dimensional, with complex classical trajectories (2) lying in the (x,z) plane. The Hamilton equations are linear, and we can find the trajectories explicitly. We can also explicitly find the tunneling exponent R [24] and analyze its dependence on the two dimensionless parameters $\omega_0\tau_0$ and $\omega_c\tau_0$, where τ_0 is the tunneling time in the absence of the magnetic field,

$$\tau_0 = 2mL/\gamma.$$

We start with the structure of the WKB action. The potential $U(\mathbf{r})$ [Eqs. (5) and (6)] has the in-plane symmetry $U(x,y,z)=U(\pm x,\pm y,z)$. It gives rise to the symmetry of the set of the Hamilton trajectories and, consequently, of the singularities of this set,

$$t\to -t^*, \quad x\to -x^*, \quad z\to z^*, \quad S\to -S^*. \qquad (17)$$

In particular, the caustic, where the outgoing wave packet and the intrawell wave function are connected, goes through the real plane (x,z) at a point $x_{\mathrm{caust}}=0$ on the symmetry axis. The z coordinate of this point depends on the magnetic field, with $z_{\mathrm{caust}}\equiv z_{\mathrm{caust}}(x=0)=L$ for $B=0$. The action for $z\leqslant z_{\mathrm{caust}}$ in the symmetry plane $x=0$ is shown in Fig. 6. As seen from the inset, the slope of the action is $\partial\,\mathrm{Im}\,S/\partial z>0$ at z_{caust}, in contrast to the 1D case where the slope is equal to zero at the turning point z_t. We note that the branches 1 and 2 are formed by the trajectories that go through real space at times $-\mathrm{Im}\,t$ being, respectively, smaller and larger than $-\mathrm{Im}\,t_{\mathrm{caust}}$ for the same trajectories [t_{caust} is given by Eq. (11)].

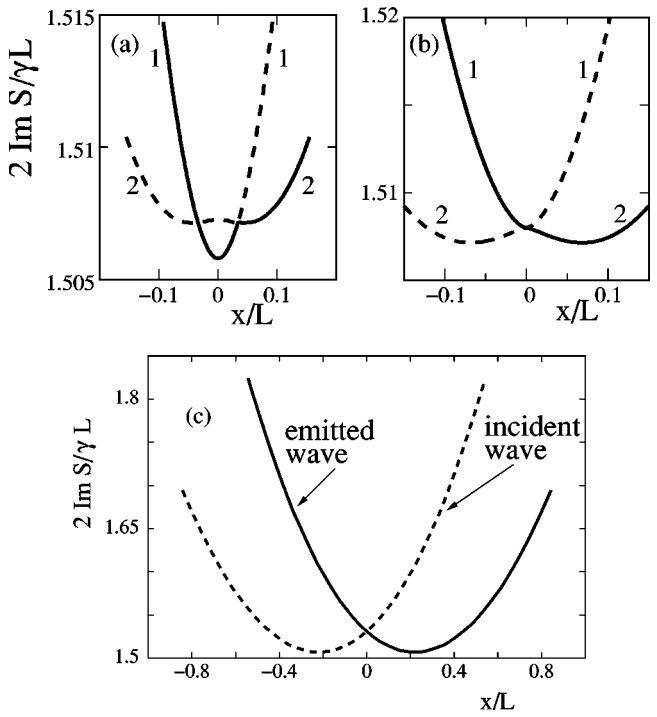

FIG. 7. Cross sections of the function $\mathrm{Im}\,S$ by the plane $z=\mathrm{const}$ in the case of tunneling in a symmetric potential (5), for (a) $z_m<z<z_{\mathrm{caust}}$, (b) $z=z_{\mathrm{caust}}$, and (c) $z>z_{\mathrm{caust}}$. The parameter values are the same as in Figs. 3 and 6. The solid lines show the branches of $\mathrm{Im}\,S$ that determine the exponent of the WKB wave function. The minima of branch 2 and of the branches in (c) have the same $\mathrm{Im}\,S$ and lie on the classical trajectory shown in Fig. 3(b).

Using the explicit form of the trajectories (2) with the initial conditions (8), one can find the complex caustic near $x=0$, $z=z_{\mathrm{caust}}\equiv z_{\mathrm{caust}}(0)$. It has the form $z_{\mathrm{caust}}(x)-z_{\mathrm{caust}}(0)=iC'x$ with real $C'/B>0$, cf. Fig. 4. It is seen from Fig. 6 that, for $x=0$, the *singular* parts of $\mathrm{Im}\,S_{1,2}$ behave as $\mp(z_{\mathrm{caust}}-z)^{3/2}$ near the caustic. Therefore we can choose the distance from the caustic in Eqs. (13)–(16) as $z'=z-z_{\mathrm{caust}}(0)-iC'x$, and the branching behavior near the caustic is then described by Fig. 5. The range $-\pi<\arg z'<0$ corresponds to real z and real positive x.

From Fig. 5, close to the caustic only one branch of the action describes the wave function for negative x and real z (the upper half of the complex z' plane). For positive x, we should keep both branches, and depending on x and z, the WKB wave function is given by the branch with the smaller $\mathrm{Im}\,S$. Near the switching line where $\mathrm{Im}\,S_1=\mathrm{Im}\,S_2$, the total wave function is given by a linear combination of the two WKB solutions.

In Fig. 6 for $z\leqslant z_{\mathrm{caust}}$, the action branch 1 describes the tail of the intrawell wave function, and the branch 2 corresponds to the wave "reflected" from the caustic. The branch 2 is nonmonotonic in z for $x=0$, with a minimum at $z_m<z_{\mathrm{caust}}$. By symmetry (17), the momentum component p_x is real for $x=0$, whereas $p_z=0$ at z_m. Therefore the point $z=z_m$, $x=0$ belongs to the classical escape trajectory shown in Fig. 3(b). Again by symmetry, this is also the point where

the escape trajectory comes most close to the well at $z=0$. However, this is not the exit point for the tunneling particle in the configuration space. Indeed, the wave function at this point is determined by the branch 1, because $\mathrm{Im}\,S_1<\mathrm{Im}\,S_2$.

Several cross sections of the action surfaces by planes $z=\mathrm{const}$ are shown in Fig. 7. For $z\leqslant z_{\mathrm{caust}}$, both branches $\mathrm{Im}\,S_{1,2}$ are symmetrical in x. However, the branch 2 is nonmonotonic in x for $z>z_m$. It has a local *maximum* at $x=0$ and two symmetrical *minima*. These minima lie on the classical trajectory shown in Fig. 3(b). For $z=z_m$, the maximum and the minima merge together. We note that at this point $\mathrm{Im}\,S_2\propto x^4$ near the minimum.

Behind the caustic in real space, $z>z_{\mathrm{caust}}$, the action $S(x,z)$ on one of the two branches is equal to $-S^*(-x,z)$ on the other branch (cf. Fig. 7). At their minima with respect to x, the values of $\mathrm{Im}\,S(x,z)$ are independent of z. These minima lie on the classical escape trajectory, as seen from the comparison with $\mathrm{Im}\,S$ for $z<z_{\mathrm{caust}}$. The branches of the action describe the incident (from large z) and emitted wave packets. Only the emitted wave is physically meaningful for the problem of tunneling escape.

As discussed above, switching between the action branches occurs for positive x where the branches of $\mathrm{Im}\,S$ cross each other. The resulting action, which determines the WKB wave function, is shown in Fig. 7 by solid lines. The switching line thus obtained coincides with the anti-Stokes switching line discussed in the preceding section.

The escaped particle can be observed as a semiclassical object if $\mathrm{Im}\,S_2(\mathbf{r}_{\mathrm{cl}})<\mathrm{Im}\,S_1(\mathbf{r}_{\mathrm{cl}})$. It ''shows up'' at the point where the classical escape trajectory intersects the switching line, cf. Fig. 3. The exit point is located for $x>0$ even though the potential (5) is symmetric. This is a consequence of the symmetry breaking by a magnetic field.

The tunneling exponent R is given by Eqs. (19) and (20) below, in which one has to set $\mu=0$. The dependence of R on $\nu_0=\omega_0\tau_0$ and $\nu_c=\omega_c\tau_0$ is shown in Fig. 8. The function R monotonically increases with the magnetic field. However, for $\omega_0\gg\omega_c,\tau_0^{-1}$ the in-plane confinement compensates the effect of the field, leading to R being nearly flat and close to its $B=0$ value of $4\gamma L/3$, as seen from Fig. 8. For weak confinement, the effect of the field becomes strong and would diverge for $\omega_c\tau_0>1$ [10,13] if ω_0 were equal to zero. For nonzero but small ω_0 (i.e., $\omega_0\tau_0\ll 1$) and for $\omega_c\tau_0-1\gg\omega_0\tau_0$ one can obtain from Eqs. (19) and (20),

$$R\approx 2\gamma L(\nu_c-1)^2(2\nu_c+1)/3\nu_c^2\nu_0.$$

The corresponding sharp increase of R with decreasing confinement frequency ω_0 and increasing ω_c is seen from Fig. 8.

The prefactor in the tunneling rate is determined by the factor $|D(\mathbf{r})|^2\propto|J^{-1}(\mathbf{r})|$ [Eqs. (1) and (12)] evaluated on the classical path $\mathbf{r}_{\mathrm{cl}}$, which should be weighted with the velocity $\dot{\mathbf{r}}_{\mathrm{cl}}$ and the factor determined by the curvature of $\mathrm{Im}\,S(\mathbf{r})$ in the direction transverse to $\dot{\mathbf{r}}_{\mathrm{cl}}$. The result is independent of a point on the path $\mathbf{r}_{\mathrm{cl}}(t)$. It could be calculated for the discussed model of the barrier complemented by a model of the intrawell potential (for example, one can use the potential for electrons on helium [11]). No interesting interference effects arise in the prefactor in this problem, in contrast to the problem of tunneling splitting in a symmetric potential in the presence of an ultrastrong magnetic field. In the latter case, tunneling is effectively one dimensional, but there may be multiple extreme paths with the same Im S. Extra phase factors have to be added when the contributions from these paths are calculated [18].

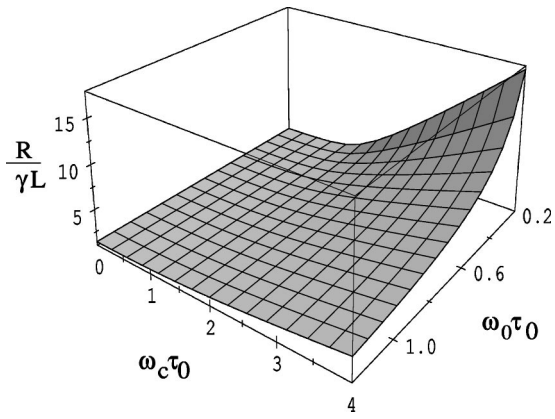

FIG. 8. The tunneling exponent R for an electron tunneling transverse to a magnetic field through the triangular potential barrier (6) as a function of the dimensionless parameters $\omega_0\tau_0$ and $\omega_c\tau_0$. In the absence of confinement in the Hall direction, i.e., for $\omega_0=0$, the tunneling exponent diverges as $\omega_c\tau_0\to 1$.

B. A nonsymmetric model

The problem considered in the preceding section for the quadratic in x,y potential $U(\mathbf{r})$ [Eq. (5)] can be solved differently. The trick is [14] to make a canonical transformation to the new coordinate p_x and the conjugate momentum $-x$. The kinetic energy then becomes $[m^2\omega_0^2x^2+p_z^2]/2m$ and is independent of the new coordinates and the magnetic field. The time-reversal symmetry is thus ''restored,'' and the problem is mapped onto the standard problem of tunneling in the 2D potential $U_0(z)+(p_x+m\omega_c z)^2/2m$.

The general method discussed in this paper is not limited to potentials with these special properties. In this section we illustrate how the method works where variables do not separate. To this end, we consider a problem of tunneling transverse to the field $\mathbf{B}\|\hat{\mathbf{y}}$ in the potential

$$U(x,z)=\frac{1}{2}m\omega_0^2x^2+\mu xz+\frac{\gamma^2}{2m}\left(1-\frac{z}{L}\right)\quad(z>0), \tag{18}$$

which differs from the potential discussed earlier by the term μxz. In the case of tunneling from a 2D electron system, this term mimics the dependence of the tunneling potential on displacements of neighboring electrons, see Appendix A.

The term μxz breaks the symmetry of the Hamilton trajectories (17). However, the Hamilton equations (2) are still linear, and we explicitly solved them. The results for $\mathrm{Im}\,S$ and the classical escape trajectory obtained using the initial conditions (8) are shown in Figs. 9 and 10. Because of bro-

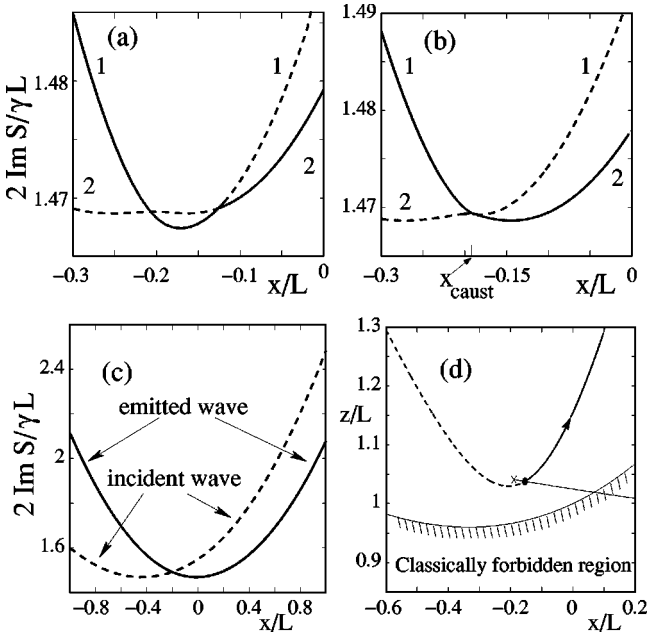

FIG. 9. Cross sections of $\mathrm{Im}\,S(x,z)$ by the plane $z=\mathrm{const}$ in the case of tunneling in the asymmetric potential $U(x,z)$ [Eq. (18)] for (a) $z_m<z<z_{\mathrm{caust}}$, (b) $z=z_{\mathrm{caust}}$, and (c) $z>z_{\mathrm{caust}}$ [at $(x_{\mathrm{caust}},z_{\mathrm{caust}})$ the caustic goes through real plane and S is branching; the corresponding point is marked by the cross in (d)]. The values of $\omega_c\tau_0$ and $\omega_0\tau_0$ are the same as in Figs. 3 and 6, and the dimensionless asymmetry parameter $\mu\tau_0^2/m=1/2$. The solid lines show the branches of $\mathrm{Im}\,S$ that determine the exponent of the WKB wave function. The minima of branch 2 lie on the classical escape trajectory shown in (d). The switching line (thin solid line) starts at the branching point.

ken symmetry, the branching point of the action in real space $(x_{\mathrm{caust}},z_{\mathrm{caust}})$, where the caustic of the set of trajectories (2) goes through real plane (x,z), lies at $x_{\mathrm{caust}}\neq 0$. It is marked by the cross in Fig. 9(d). Its position depends on μ and other parameters of the system. Similarly, the time where the caustic crosses the real space has both real and imaginary parts, in contrast to the case $\mu=0$ where it was purely imaginary, see Fig. 3.

For $\mu\neq 0$, the surfaces $\mathrm{Im}\,S(x,z)$ become asymmetric. The general structure of the solution, however, remains the same as in the case $\mu=0$. This can be seen by comparing the cross sections of the action in Figs. 7 and 9. In both figures, the cross sections in (a), (b), and (c) refer to the planes $z<z_{\mathrm{caust}}$, $z=z_{\mathrm{caust}}$, and $z>z_{\mathrm{caust}}$, respectively. As in the symmetrical case, the branches 1 and 2 for $\mu\neq 0$ are formed

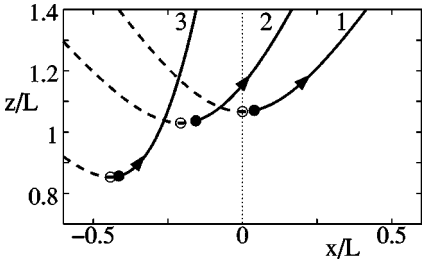

FIG. 10. Classical escape trajectories. The dimensionless asymmetry parameter on the curves 1–3 is $\mu\tau_0^2/m=0,0.5,1.5$. The filled circles are exit points and the open circles are the points z_m where the trajectory is closest to the localized state.

by the trajectories in complex time t, with $-\mathrm{Im}\,t$ being, respectively, smaller and bigger than $-\mathrm{Im}\,t_{\mathrm{caust}}$. At the point $(x_{\mathrm{caust}},z_{\mathrm{caust}})$, branches 1 and 2 touch each other.

Switching between the branches in real space occurs for $z<z_{\mathrm{caust}}$. It can be analyzed in the same way as for $\mu=0$. The WKB wave function is determined by the branch in Fig. 9 shown with the solid line. The switching line starts from the branching point $(x_{\mathrm{caust}},z_{\mathrm{caust}})$ and goes in the direction of positive x.

Branch 2 has two minima as a function of x for $z_m<z<z_{\mathrm{caust}}$. It is asymmetric for $\mu\neq 0$. However, the minimal values of $\mathrm{Im}\,S$ remain equal to each other and are the same in all cross sections $z=\mathrm{const}$. The minima of $\mathrm{Im}\,S$ lie on the classical trajectory along which the electron escapes. At $x=x_m, z=z_m$ they merge together, and $\mathrm{Im}\,S$ becomes quartic in $x-x_m$. The value z_m shows how close the escape trajectory comes to the localized intrawell state.

The classical trajectory becomes observable in configuration space once it crosses the switching line. The shape of the trajectory and the exit point for several values of the asymmetry parameter μ are shown in Fig. 10. The outgoing wave packet is Gaussian near the maximum ($\mathrm{Im}\,S$ is parabolic near the corresponding minimum).

By solving the Hamilton equations (2) for the potential (18), we can write the tunneling exponent (10) in the form

$$R=2\gamma L[\tau_{\mathrm{rd}}+\nu_0\kappa(\tau_{\mathrm{rd}})]. \tag{19}$$

Here, τ_{rd} is the imaginary part of the time to reach the classical escape trajectory [see Fig. 3(a)] in the units of the tunneling time τ_0 for $B=\mu=0$. Along with the function κ in Eq. (19), the reduced time τ_{rd} can be found from the equation

$$\kappa(\tau_{\mathrm{rd}})\equiv\frac{\nu_0^2(\tau_{\mathrm{rd}}\cos\nu_-\tau_{\mathrm{rd}}-\nu_-^{-1}\sin\nu_-\tau_{\mathrm{rd}})+\nu_-^2\cos\nu_-\tau_{\mathrm{rd}}-\nu_-(1-\nu_0+\nu_0\tau_{\mathrm{rd}})\sin\nu_-\tau_{\mathrm{rd}}}{\tilde{\mu}^2(\nu_0\cos\nu_-\tau_{\mathrm{rd}}-\nu_-\sin\nu_-\tau_{\mathrm{rd}})}$$

$$=\frac{(\nu_0^2\tau_{\mathrm{rd}}-\nu_+^2)\cosh\nu_+\tau_{\mathrm{rd}}+\nu_+(1-\nu_0+\nu_0\tau_{\mathrm{rd}}-\nu_0^2/\nu_+^2)\sinh\nu_+\tau_{\mathrm{rd}}}{\tilde{\mu}^2(\nu_0\cosh\nu_+\tau_{\mathrm{rd}}+\nu_+\sinh\nu_+\tau_{\mathrm{rd}})}. \tag{20}$$

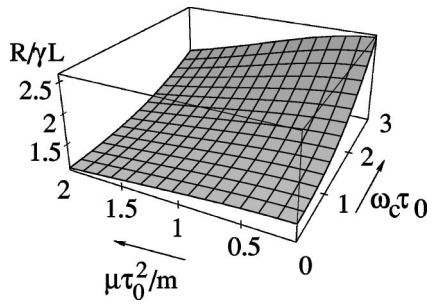

FIG. 11. The tunneling exponent R as a function of the magnetic field and the asymmetry parameter μ in the model (18) for $\omega_0\tau_0=1.2$. The function R is even in μ.

Here, $\tilde{\mu}=\mu\tau_0^2/m$ is the dimensionless asymmetry parameter. The motion under the barrier is characterized by the dimensionless frequencies $\nu_0=\omega_0\tau_0$, $\nu_c=\omega_c\tau_0$, and their combinations $\nu=(\nu_c^2+\nu_0^2)^{1/2}$ and $\nu_\pm{}^2=\pm\nu^2/2+\sqrt{\nu^4/4+\tilde{\mu}^2}$.

The tunneling exponent R depends on the interrelation between the in-plane electron dynamics, which is characterized by the frequency ω_0, the cyclotron frequency ω_c, the tunneling time τ_0, and the asymmetry parameter μ. The exponent R increases with the magnetic field. The dependence of R on ω_c,ω_0 for $\mu=0$ as given by Eqs. (19) and (20) is shown in Fig. 8. A typical dependence of R on μ and B for $\omega_0\tau_0\sim 1$ is shown in Fig. 11.

The asymmetry results in lowering of the tunneling barrier for $B=0$ and the corresponding increase of the tunneling rate. This can be qualitatively understood, since a displacement in the x direction with $\mu x<0$ increases the effective force in the z direction, which pulls the electron away from the layer. For small asymmetry, $\tilde{\mu}\ll 1$, the correction to R is quadratic in $\tilde{\mu}$. In the limit of a thin and high tunneling barrier for $x=0$ or soft in-plane vibrations, where $\omega_0\tau_0\ll 1$, tunneling is most likely to occur in the barrier, which is adiabatically prepared by the optimal in-plane displacement x (the ''completely adjusted'' barrier [36]). The expression for R takes a form

$$R=2\gamma L(3\nu_0/\tilde{\mu}^2)^{1/3} \quad (\nu_0=\omega_0\tau_0\ll 1), \tag{21}$$

it depends on the in-plane frequency ω_0 and on μ nonanalytically. The role of the asymmetry increases with the magnetic field, as seen from Fig. 11.

In terms of comparison with the currently available experimental data on tunneling from a correlated 2D many-electron system on helium surface [10], of utmost interest is the situation where the asymmetry is small. For B parallel to the electron layer, the observed dependence of R on B did not show the divergence expected if the tunneling electron were free to move along the layer. The simple model (5) provides a qualitative explanation of the experiment [24]. Excellent quantitative agreement, without adjustable parameters, was achieved by using a dynamical model of the correlated system, which can be efficiently mimicked by Eq. (5) and also incorporates the curvature of the potential $U_0(z)$ due to electron correlations [11].

VI. THE PATH-INTEGRAL FORMULATION IN A MAGNETIC FIELD

In the absence of a magnetic field, the problem of tunneling decay is often considered using the instanton technique [25,26]. This technique applies if the potential well is parabolic near the minimum and thermalization inside the well occurs much faster than escape from the well (in the case of 2D electron systems, both conditions are often violated [11]). Because the Schrödinger equation for metastable states has to be solved with the radiation boundary condition, the energies of these states acquire small imaginary parts, and so does the partition function Z. The escape rate W for finite temperatures is simply related to $\mathrm{Im}\,Z$,

$$W\approx 2T\,\mathrm{Im}\,Z/\mathrm{Re}\,Z \tag{22}$$

(we have set $k_B=1$).

The partition function is given by the integral over periodic paths $\mathbf{r}(\tau)$ in imaginary time [37],

$$Z=\int_{\mathbf{r}(0)=\mathbf{r}(\beta)}\mathcal{D}\mathbf{r}(\tau)\exp\{-S_E[\mathbf{r}(\tau)]\}, \tag{23}$$

where $\beta=T^{-1}$ and S_E is the Euclidean action (the action in imaginary time). It is real for $B=0$ and for real trajectories $\mathbf{r}(\tau)$.

The general expressions (22) and (23) should also apply in the presence of a magnetic field. However, the Euclidean action for an electron

$$S_E=\int_0^\beta d\tau\left[\frac{m}{2}\left(\frac{d\mathbf{r}}{d\tau}\right)^2+U(\mathbf{r})+i\frac{e}{c}\mathbf{A}(\mathbf{r})\frac{d\mathbf{r}}{d\tau}\right] \tag{24}$$

is now complex. Therefore the standard way [25,26] of evaluating the escape rate has to be revised, except for special symmetric cases like that discussed in Sec. V A, where one can change to new variables in which S_E becomes real [14,16].

The goal of this section is to show how the instanton technique works in the case of a complex action functional. Although we will often refer to the action functional of the form (24), much of the results below apply also to a more general retarded Euclidean action, which is of interest for systems coupled to a bath.

In the spirit of the WKB approximation, the path integral (23) will be evaluated by the steepest-descent method in the one-bounce approximation. The extremal paths $\mathbf{r}(\tau)$ of the functional S_E satisfy the equation

$$m\frac{d^2\mathbf{r}}{d\tau^2}=\boldsymbol{\nabla}U(\mathbf{r})+i\frac{e}{c}\left[\frac{d\mathbf{r}}{d\tau}\times\mathbf{B}\right]. \tag{25}$$

This equation has to be solved with the periodic boundary condition $\mathbf{r}(0)=\mathbf{r}(\beta)$. Note that the sign of the potential has been inverted compared to the case of classical motion in real time.

For low temperatures and for the potential $U(\mathbf{r})$, which is parabolic near its intrawell minimum $\mathbf{r}_{\mathrm{well}}$, Eq. (25) has a solution $\mathbf{r}(\tau)=\mathbf{r}_{\mathrm{well}}$, with $S_E=0$. It gives the real part of the

partition function, see below. As in the case $B=0$, the imaginary part of Z is determined by another solution of Eq. (25), which is of the bounce type. This solution, $\mathbf{r}_b(\tau)$, starts near $\mathbf{r}_{\rm well}$, slides downhill in the inverted potential $-U(\mathbf{r})$, and in time β comes back. For $B=0$ the corresponding path is a symmetric real trajectory, $\mathbf{r}_b(\tau)=\mathbf{r}_b(\beta-\tau)$, which bounces off the turning point $\dot{\mathbf{r}}_b(\beta/2)=0$.

For $B\neq 0$, because of broken time-reversal symmetry, the path $\mathbf{r}_b(\tau)$ is complex, and the velocity along this path does not become equal to zero. The path is not symmetrical in time, because the replacement $\tau\to-\tau$ changes Eq. (25). However, if we simultaneously change $i\to-i$, the equation remains unchanged. Therefore the bounce-type path has the symmetry

$$\mathbf{r}_b(\tau)=\mathbf{r}_b^*(\beta-\tau). \tag{26}$$

An immediate and very important consequence of Eq. (26) is that the value of $S_E(\mathbf{r}_b)$ for the bounce-type path is *real*. This value gives the tunneling exponent.

A. The eigenvalue problem

The prefactor in Z can be found by integrating over the tubes of paths around the extremal paths. It can be done by expanding S_E in deviations from the extremal paths to the second order, and then expanding $\mathbf{r}(\tau)-\mathbf{r}_{\rm well}$ and $\mathbf{r}(\tau)-\mathbf{r}_b(\tau)$ in the three-vector eigenfunctions $\boldsymbol{\psi}_n(\tau)$ of the appropriate eigenvalue problem,

$$\hat{\mathcal{F}}\boldsymbol{\psi}_n\equiv\int_0^\beta d\tau'\,\hat{\mathbf{F}}(\tau,\tau')\,\boldsymbol{\psi}_n(\tau')=\lambda_n\boldsymbol{\psi}_n(\tau),$$
$$\hat{F}_{ij}(\tau,\tau')=\delta^2 S_E/\delta r_i(\tau)\,\delta r_j(\tau'). \tag{27}$$

Here, the derivatives of the action are calculated on the corresponding extremal trajectory $\mathbf{r}_{\rm well}$ and $\mathbf{r}_b(\tau)$, and periodic boundary conditions are assumed. The operator $\hat{F}$ is simplified for a nonretarded action (24), $\hat{F}_{ij}(\tau,\tau')=\delta(\tau-\tau')\hat{\mathrm{f}}_{ij}(\tau)$.

For $B=0$, the operator $\hat{\mathcal{F}}$ is Hermitian, with $\hat{\mathrm{f}}_{ij}=-m\delta_{ij}(d^2/d\tau^2)+\partial^2U/\partial r_i\partial r_j$, if the action is given by Eq. (24). Therefore the functions $\boldsymbol{\psi}_n(\tau)$ form complete and orthogonal sets for each extreme trajectory (25), and the eigenvalues λ_n are real.

For $B\neq 0$, the operator $\hat{\mathcal{F}}$ becomes non-Hermitian. For example, in the case of a uniform magnetic field in Eq. (24), $\hat{\mathrm{f}}_{kl}(\tau)$ acquires an extra term $i(e/c)\epsilon_{klj}B_j(d/d\tau)$ (ϵ_{klj} is the Levi-Civita symbol). Therefore some of the eigenvalues λ_n become complex. The eigenvectors $\boldsymbol{\psi}_n$ with different n are orthogonal not to each other, but to the eigenvectors $\boldsymbol{\phi}_n$ of the Hermitian conjugate operator,

$$\int_0^\beta d\tau'\,\hat{\mathbf{F}}^\dagger(\tau,\tau')\,\boldsymbol{\phi}_n(\tau')=\lambda_n^*\boldsymbol{\phi}_n(\tau).$$

Taking into account the symmetry (26) of the extremal trajectories, we find that

$$\hat{\mathbf{F}}^\dagger(\tau,\tau')=\hat{\mathbf{F}}(\beta-\tau,\beta-\tau')=\hat{\mathbf{F}}^*(\tau,\tau'). \tag{28}$$

The energy spectra for several complex Hamiltonians with symmetry similar to Eq. (28) (called the $\mathcal{PT}$ symmetry) were investigated earlier numerically and using the WKB approximation [38].

The symmetry (28) has several consequences. First, it shows that $\boldsymbol{\psi}_n(\tau)=\alpha_n\boldsymbol{\phi}_n^*(\tau)$, where α_n is a constant. This means that, with proper normalization, the orthogonality relation becomes

$$\int_0^\beta d\tau\,\boldsymbol{\psi}_m(\tau)\,\boldsymbol{\psi}_n(\tau)=\delta_{mn} \tag{29}$$

[here, we assumed that the eigenvalues are nondegenerate; for degenerate eigenvalues, the condition (29) can be satisfied by choosing appropriate linear combinations of the eigenfunctions with same λ_n].

It also follows from Eq. (28) that, if $\boldsymbol{\psi}_n(\tau)$ is an eigenfunction of Eq. (27) with an eigenvalue λ_n, then $\boldsymbol{\psi}_n^*(\beta-\tau)$ is also an eigenfunction of the same boundary-value problem, but with the eigenvalue λ_n^*. This means that the eigenvalues λ_n are either real or form pairs of complex-conjugate numbers.

Pairs of complex-conjugate eigenvalues emerge in the following way. For $B=0$, all eigenvalues are real. With increasing B some eigenvalues approach each other pairwise, while still remaining real. Eventually they merge, and for larger B become complex conjugate. Such behavior with varying control parameter is generic for systems with symmetry (28), as described in Appendix B. For 1D Schrödinger-type equations with different complex Hamiltonians it was observed numerically [38].

1. Eigenvalues near the potential well

As an illustration, we consider the eigenvalue problem near $\mathbf{r}_{\rm well}$ for the action functional (24). Here, Eq. (27) becomes linear, and the eigenfunctions $\boldsymbol{\psi}_n(\tau)$ can be sought in the form of linear combinations of $\exp(\pm i\omega_n\tau)$, with $\omega_n=2\pi n/\beta$. The eigenvalues are obtained from the equation

$$\det\left[(m\omega_n^2-\lambda_{n\nu})\,\delta_{kl}+m\Omega_{kl}^2-\frac{e}{c}\,\omega_n\epsilon_{klj}B_j\right]=0, \tag{30}$$

where $m\Omega_{kl}^2=[\partial^2U/\partial r_k\partial r_l]_{\mathbf{r}_{\rm well}}$ and $\mathbf{B}$ is the magnetic field at $\mathbf{r}_{\rm well}$. The subscript ν enumerates the eigenvalues λ for a given Matsubara frequency.

If, for example, $\mathbf{B}$ is pointing along a principal axes of the tensor Ω_{kl}^2 (say, the axes 1), then we have $\lambda_{n\,1}/m=\omega_n^2+\Omega_1^2$, and

$$m^{-1}\lambda_{n2,3}=\omega_n^2+\frac{1}{2}(\Omega_2^2+\Omega_3^2)\pm\frac{1}{2}[(\Omega_2^2-\Omega_3^2)^2-4\omega_c^2\omega_n^2]^{1/2}, \tag{31}$$

where $\Omega_\nu^2>0$ are the principal values of the tensor Ω_{kl}^2. Clearly, the eigenvalues $\lambda_{n2,3}$ are complex-conjugate pairs for large enough $\omega_n^2\omega_c^2$.

Equation (31) shows explicitly also how pairs of complex eigenvalues emerge with varying magnetic field as a result of merging of adjacent real eigenvalues, as discussed for the general case in Appendix B.

2. Eigenvalues for the bounce trajectory

A specific feature of the eigenvalue problem (27) for the bounce trajectory $\mathbf{r}_b(\tau)$ at low temperatures is that one of the eigenvalues is $\lambda_1^{(b)}=0$. It corresponds to the eigenfunction $\boldsymbol{\psi}_1(\tau)\propto\dot{\mathbf{r}}_b(\tau)$. For $B=0$, the vector function $\boldsymbol{\psi}_1(\tau)\propto\dot{\mathbf{r}}_b(\tau)$ has one zero for all components. Therefore it is the eigenfunction of the first excited state of the multicomponent (but still one-dimensional, with ''coordinate'' τ) Schrödinger-type equation (27). Since the eigenvalue problem (27) is Hermitian for $B=0$, by oscillation theorem all eigenvalues $\lambda_n^{(b)}$ with $n\geqslant 2$ are positive, and the eigenvalue of the ground state is negative, $\lambda_0^{(b)}<0$ [25].

We are not aware of the oscillation theorem for non-Hermitian problems. However, $\boldsymbol{\psi}_1(\tau)\propto\dot{\mathbf{r}}_b(\tau)$ is still an eigenfunction for $B\neq 0$, and $\lambda_1^{(b)}=0$. Therefore it follows from arguments in Appendix B that, as B increases from zero, the eigenvalue $\lambda_1^{(b)}$ does not merge with other real eigenvalues to form a pair of complex-conjugate eigenvalues. As a consequence, pairs of complex-conjugate eigenvalues will be formed only from the $\lambda_n^{(b)}$ that were positive for $B=0$. The negative root $\lambda_0^{(b)}$ will remain real and negative. In principle, as a result of coalescence of complex-conjugate eigenvalues, there may emerge pairs of negative real eigenvalues, and then they can further bifurcate into complex pairs. However, the total number of negative real eigenvalues will be odd.

B. The prefactor in the tunneling rate

We are now in a position to discuss the prefactor in the partition function Z. The standard step is to expand the deviation $\delta\mathbf{r}(\tau)$ of the integration path in Eq. (23) from the extreme trajectory $\mathbf{r}_{\rm well}$ or $\mathbf{r}_{\rm b}$ in terms of the eigenfunctions $\boldsymbol{\psi}_n$ of the corresponding eigenvalue problem, $\delta\mathbf{r}(\tau)=\Sigma c_n\boldsymbol{\psi}_n(\tau)$. With account taken of the orthogonality condition (29), the increment δS_E of the Euclidean action related to the deviation of the trajectory $\delta\mathbf{r}$ then becomes $\delta S_E=\Sigma\lambda_n c_n^2/2$.

The above expansion assumes that the set $\{\boldsymbol{\psi}_n\}$ is complete. The completeness is known for $B=0$, where the eigenvalue problem (27) is Hermitian. As B changes, the number of states does not change. From the orthogonality condition (29), none of the eigenfunctions becomes a linear combination of other eigenfunctions. This makes us believe that the functions $\boldsymbol{\psi}_n$ form a complete set even for $B\neq 0$ and justifies the above expansion.

The path integral (23) can be obtained as a limit $N\to\infty$ of integrals over $d\mathbf{r}(\tau_k)$ at discretized instants of time $\tau_k=k\Delta\tau,\Delta\tau=\beta/N$. In the standard way, we change to integration over dc_n. Because of the orthogonality relation (29), the determinant $\det[\boldsymbol{\psi}_n(\tau_k)]$ of the transformation of variables is real and is equal to $\pm(\Delta\tau)^{-N/2}$. Integration of $\exp(-\delta S_E)$ over dc_n gives const$\times\Pi_n\lambda_n^{-1/2}$.

Let us now consider the contribution to the partition function $Z_{\rm well}$ from trajectories close to the potential minimum $\mathbf{r}_{\rm well}$. The corresponding eigenvalues $\lambda_n^{(\rm well)}$ are either positive or belong to complex conjugate pairs, cf. Eq. (31). Therefore $Z_{\rm well}$ is real. Since $S_E[\mathbf{r}_{\rm well}]=0$, there is no exponentially small factor in $Z_{\rm well}$. This term gives the partition function for low-lying intrawell excitations in the presence of the magnetic field.

When evaluating the contribution $Z_{\rm b}$ from paths close to the bounce trajectory, special care has to be taken of the eigenvalue $\lambda_1^{(b)}=0$. A standard analysis [25,26] shows that integration over dc_1 gives the factor β in $Z_{\rm b}$. The positive and complex-conjugate eigenvalues $\lambda_n^{(b)}$ give a real positive factor in $Z_{\rm b}$, whereas the negative eigenvalues $\lambda_0^{(b)}$ (or an odd number of negative eigenvalues) make $Z_{\rm b}$ purely imaginary. In addition, $Z_{\rm b}$ contains the exponential factor $\exp(-S_E[\mathbf{r}_{\rm b}(\tau)])$. Overall, this gives the tunneling rate (22),

$$W\approx 2T|Z_{\rm b}|/Z_{\rm well}\propto\exp\{-S_E[\mathbf{r}_{\rm b}(\tau)]\}. \tag{32}$$

Equation (32) shows that the instanton technique can be applied to the problem of tunneling decay in the presence of a magnetic field in spite of the field-induced breaking of time-reversal symmetry. Although the instanton action remains real, the actual calculation is very different from that for $B=0$. Also, the bounce trajectory touches the classical escape trajectory at a point $\mathbf{r}_{\rm b}(\beta/2)$, which is not the point where the particle ''shows up'' as a semiclassical wave packet; the latter point can be found from our general WKB analysis of tunneling decay.

VII. CONCLUSIONS

In conclusion, the problem of tunneling decay in a magnetic field can be solved in the semiclassical limit by analyzing the Hamilton trajectories of the particle in complex phase space and time. The boundary conditions are determined by the intrawell wave function and its analytic continuation. This approach allows one to find both the tunneling exponent and the tail of the wave function of the localized state. It does not require to consider either a part of the potential or the magnetic field as a perturbation, and it can be applied to a three-dimensional potential of a general form. The multidimensional character of the problem is important. In particular, confinement in the Hall direction (transverse to the directions of tunneling and the magnetic field) can exponentially strongly increase the tunneling rate by reducing the Hall velocity.

The escape rate in a magnetic field is generally *exponentially* smaller than the probability for a particle to reach the boundary of the classically accessible range $U(\mathbf{r})=E$. The escaped particle ''shows up'' from the tunneling barrier with nonzero velocity and behind the surface $U(\mathbf{r})=E$. The connection of the decaying and propagating waves occurs on caustics of the set of complex Hamilton trajectories, where the classical action is branching. Caustics are complex surfaces in 3D space. In the presence of a magnetic field, they go through real space along lines (instead of surfaces, for $B=0$).

An interesting feature of tunneling in a magnetic field is the occurrence of a switching surface, where different WKB branches of the wave function have same amplitudes. The slope of the *logarithm* of the wave function normal to the surface sharply changes there, from the value on one of the branches to that on the other branch. The escaped particle first shows up as a propagating semiclassical wave packet on the switching surface where the classical escape trajectory crosses it. Switching surfaces can be observed by measuring the electron-density distribution behind the potential barrier. A simpler experiment will be to investigate the dependence of the classical escape trajectory behind the barrier on a magnetic field. This trajectory is sensitive to the form of the effective confining potential, which is particularly interesting where this potential mimics many-body effects in correlated systems.

Switching between branches of the WKB wave function for $B \neq 0$ is similar to switching between different branches of the probability distribution in classical systems away from thermal equilibrium. Such systems lack time-reversal symmetry, as do also quantum systems in a magnetic field. Tails of the classical distributions are formed by infrequent fluctuations. Fluctuational paths to a given state from the vicinity of an equilibrium position (attractor) form a narrow tube centered at the most probable path. This path is given by a solution of the variational problem of finding the maximum of the logarithm of the probability distribution [39–41]. In many cases of physical interest the corresponding Euler equations are similar to Eqs. (2). However, in contrast to underbarrier tunneling trajectories, classical optimal paths can be observed [42]. Switching surfaces in the phase space of fluctuating nonequilibrium systems separate areas reached along topologically different optimal paths [43a]. They have been seen in analog simulations [43b].

It follows from the results of this paper that for potential wells that are parabolic near the minimum, even in the presence of a magnetic field one can still use the instanton technique in order to find the escape rate. However, the bounce trajectory, which gives the tunneling exponent, is now complex. Also in contrast to the $B=0$ case, evaluation of the prefactor requires solving a non-Hermitian boundary-value problem. Because of special symmetry of this problem (which is the same as the $\mathcal{PT}$ symmetry discussed previously for 1D complex Hamiltonians [38]), the corresponding eigenvalues are either real or form pairs of complex-conjugate numbers.

Our results for the model that mimics tunneling from a strongly correlated 2D electron system illustrate the general conclusions about tunneling in a magnetic field, including the structure of singularities related to branching of the WKB wave function and the occurrence of switching surfaces. They show that the rate of tunneling transverse to the magnetic field is highly sensitive to the in-plane electron dynamics and exponentially increases when electrons are more strongly confined in the plane, i.e., the frequencies of in-plane vibrations increase. It also increases if electrons in the 2D layer can adjust to the tunneling electron and thus effectively decrease its tunneling barrier.

ACKNOWLEDGMENT

This research was supported in part by the NSF through Grant Nos. PHY-0071059 and ITR/RC-0085922.

APPENDIX A: THE MANY-ELECTRON HAMILTONIAN

A simple and important model that allows us to consider the effect of electron correlations on tunneling from a 2D electron system is the model of a Wigner crystal. In this model, the in-plane electron motion is small-amplitude vibrations about equilibrium positions. Because of strong correlations, exchange effects are not important, and the tunneling electron can be identified. Its tunneling motion is affected by the interaction with other electrons.

We will assume that the equilibrium in-plane position of the tunneling electron is at the origin. Then, in the presence of a magnetic field **B** parallel to the electron layer, the full Hamiltonian is of the form

$$H = \frac{p_z^2}{2m} + U_0(z) + H_v + H_B, \tag{A1}$$

with

$$H_v = \frac{1}{2} \sum_{\mathbf{k},j} \left[m^{-1} \mathbf{p}_{\mathbf{k}j} \mathbf{p}_{-\mathbf{k}j} + m \omega_{\mathbf{k}j}^2 \mathbf{u}_{\mathbf{k}j} \mathbf{u}_{-\mathbf{k}j} \right] \tag{A2}$$

and

$$H_B = \frac{1}{2} m \omega_c^2 z^2 - \omega_c z N^{-1/2} \sum_{\mathbf{k},j} \left[\hat{\mathbf{B}} \times \mathbf{p}_{\mathbf{k}j} \right]_z + U_{\mathrm{int}}(z, \{\mathbf{u}_{\mathbf{k}j}\}). \tag{A3}$$

Here, $\mathbf{p}_{\mathbf{k}j}$, $\mathbf{u}_{\mathbf{k}j}$, and $\omega_{\mathbf{k}j}$ are the 2D momentum, displacement, and frequency of the Wigner crystal phonon of branch $j (j=1,2)$ with 2D wave vector $\mathbf{k}$. The in-plane momentum of the tunneling electron is $N^{-1/2} \Sigma \mathbf{p}_{\mathbf{k}j}$ (N is the number of electrons). The term $U_0(z)$ describes the tunneling barrier [cf. Eq. (6)] for the electron at the origin provided all other electrons are at their in-plane lattice sites.

The term H_B couples the out-of-plane tunneling motion to lattice vibrations. The problem of many-electron tunneling is thus mapped onto a familiar problem of a particle coupled to a bath of harmonic oscillators [14,37]. A part of the coupling is due purely to the magnetic field. Another part comes from the term U_{int}, which describes the change of the tunneling barrier because of electron vibrations. Its simplest form is given by the lowest-order term of the expansion of the electron energy,

$$U_{\mathrm{int}}(z, \{\mathbf{u}_{\mathbf{k}j}\}) = z \sum_{\mathbf{k},j} \mathbf{g}_{-\mathbf{k}j} \mathbf{u}_{\mathbf{k}j}, \tag{A4}$$

where $\mathbf{g}_{\mathbf{k}j}$ are coupling constants (for electrons on a thick helium film [36] the leading term in U_{int} is $\propto z^2$). The coupling (A4) leads to lowering of the tunneling barrier as a result of appropriate displacements of the electrons surrounding the tunneling electron.

The major effect on tunneling comes from high-frequency in-plane vibrations, which have large density of states [11]. Therefore it is not unreasonable to use the Einstein model of the Wigner crystal, in which all vibrations have the same frequency ω_0. Then, except for the term $U_{\rm int}$, the Hamiltonian (A1) becomes a sum of Hamiltonians of confined noninteracting electrons of the form (3), with the potential $U(\mathbf{r})$ given by Eq. (5). This explains why Eqs. (3) and (5) can be used to mimic the effect of electron correlations on tunneling.

In the Einstein model, because of the symmetry of a 2D Wigner crystal, there is no coupling term in $U_{\rm int}$ that would be linear in the in-plane displacement of the tunneling electron itself. Instead, for $B=0$ its out-of-plane motion is coupled to an in-plane oscillator with the coordinate given by a (totally symmetric) linear combination of displacements of other electrons. This maps the problem onto the problem discussed in Sec. V B, with the in-plane electron coordinate x in Eq. (18) corresponding to the coordinate of this oscillator, and with μ being a linear combination of the (weighted) coefficients $\mathbf{g}_{\mathbf{k}j}$. For $B\neq 0$, the coupling of tunneling motion to in-plane vibrations of the tunneling electron itself [the second term in Eq. (A3)] also becomes substantial. Yet we expect that the model (18) catches important qualitative features of many-electron tunneling even where both the magnetic field and the interaction $U_{\rm int}$ are substantial.

APPENDIX B: EMERGENCE OF COMPLEX EIGENVALUES

In this appendix we consider how, with the varying control parameter, two real eigenvalues of the problem (27) merge and then become complex. Near this bifurcation, the eigenvalues can be sought by perturbation theory. We start with a value of $\mathbf{B}=\mathbf{B}_0$ (we can also use another control parameter), where the given adjacent eigenvalues λ_n,λ_m are close to each other and are real. For small $|\delta\mathbf{B}|=|\mathbf{B}-\mathbf{B}_0|$, the functional $\hat{\mathcal{F}}$ is close to its value for $\mathbf{B}_0$, $\hat{\mathcal{F}}\approx\hat{\mathcal{F}}_0+\delta\hat{\mathcal{F}}$ in Eq. (27). To first order in $\delta\hat{\mathcal{F}}$, the eigenvalues are given by the expressions $[\lambda_n(\mathbf{B}_0)+\lambda_m(\mathbf{B}_0)]/2+\lambda_\pm$, with

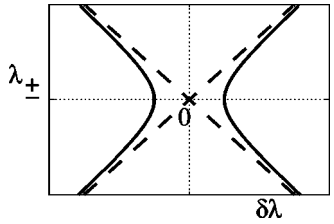

FIG. 12. The dependence of the eigenvalue shifts $\lambda_\pm$ on the distance $\delta\lambda$ between the eigenvalues for $\mathbf{B}=\mathbf{B}_0$ (schematically). We count $\delta\lambda$ off from $\delta\hat{\mathcal{F}}^{nn}-\delta\hat{\mathcal{F}}^{mm}$, and $\lambda_\pm$ from $(\delta\hat{\mathcal{F}}^{nn}+\delta\hat{\mathcal{F}}^{mm})/2$.

$$\lambda_\pm=\frac{1}{2}(\delta\hat{\mathcal{F}}^{nn}+\delta\hat{\mathcal{F}}^{mm})\pm\frac{1}{2}[(\delta\hat{\mathcal{F}}^{nn}-\delta\hat{\mathcal{F}}^{mm}-\delta\lambda)^2+4\,\delta\hat{\mathcal{F}}^{nm}\delta\hat{\mathcal{F}}^{mn}]^{1/2},\quad \delta\hat{\mathcal{F}}^{nm}=\langle\psi_n|\,\delta\hat{\mathcal{F}}|\psi_m\rangle. \quad \text{(B1)}$$

Here, the wave functions are calculated for $\mathbf{B}_0$, and $\delta\lambda=\lambda_m-\lambda_n$.

Because of the symmetry (28), the matrix elements of $\delta\hat{\mathcal{F}}$ in Eq. (B1) are real. However, the product $\delta\hat{\mathcal{F}}^{nm}\delta\hat{\mathcal{F}}^{mn}$ does not have to be positive, and in fact we are interested in the case where it is negative. In this case, instead of level anticrossing, we have the dependence of the eigenvalues on the distance $\delta\lambda$ shown in Fig. 12. In the gap, the eigenvalues are complex conjugate.

The control parameter in the tunneling problem is not $\delta\lambda$, and it may be more interesting to look at the eigenvalues as functions of $\delta\hat{\mathcal{F}}^{nm}$. Their behavior is similar to what is shown in Fig. 12, if the diagonal and off-diagonal matrix elements depend on the control parameter (for example, the magnetic field) in the same way. Otherwise, once the eigenvalues become complex with changing control parameter, they do not have to become real again, as is the case for the eigenvalues given by Eqs. (31) as functions of ω_c. We note that there is also an opposite process of merging of complex-conjugate eigenvalues, which is also described by Eq. (B1).

[1] B. I. Shklovskii and A. L. Efros, *Electronic Properties of Doped Semiconductors* (Springer-Verlag, New York, 1984).

[2] For reviews, see J. P. Eisenstein, in *Perspectives in Quantum Hall Effects*, edited by S. Das Sarma and A. Pinczuk (Wiley, New York, 1997), p. 37; C. L. Kane and M. P. A. Fisher, *ibid.*, p. 109; S. M. Girvin and A. H. MacDonald, *ibid.*, p. 161; B. I. Halperin, *ibid.*, p. 225.

[3] N. B. Zhitenev, M. Brodsky, R. C. Ashoori, and M. R. Melloch, Phys. Rev. Lett. **77**, 1833 (1996); M. B. Hastings and L. S. Levitov, *ibid.* **77**, 4422 (1996).

[4] M. Grayson, D. C. Tsui, L. N. Pfeiffer, K. W. West, and A. M. Chang, Phys. Rev. Lett. **86**, 2645 (2001), and references therein.

[5] I. B. Spielman, J. P. Eisenstein, L. N. Pfeiffer, and K. W. West, Phys. Rev. Lett. **84**, 5808 (2000).

[6] J. Smoliner, W. Demmerle, G. Berthold, E. Gornik, G. Weimann, and W. Schlapp, Phys. Rev. Lett. **63**, 2116 (1989); G. Rainer, J. Smoliner, E. Gornik, G. Böhm, and G. Weimann, Phys. Rev. B **51**, 17 642 (1995).

[7] J. P. Eisenstein, T. J. Gramila, L. N. Pfeiffer, and K. W. West, Phys. Rev. B **44**, 6511 (1991); S. Q. Murphy, J. P. Eisenstein, L. N. Pfeiffer, and K. W. West, *ibid.* **52**, 14 825 (1995).

[8] L. Zheng and A. H. MacDonald, Phys. Rev. B **47**, 10 619 (1993).

[9] T. Ihn, H. Carmona, P. C. Main, L. Eaves, and M. Henini, Phys. Rev. B **54**, R2315 (1996); M. J. Yang, C. H. Yang, B. R. Bennett, and B. V. Shanabrook, Phys. Rev. Lett. **78**, 4613 (1997); M. Lakrimi, S. Khym, R. J. Nicholas, D. M. Symons, F. M. Peeters, N. J. Mason, and P. J. Walker, *ibid.* **79**, 3034 (1997).

[10] L. Menna, S. Yücel, and E. Y. Andrei, Phys. Rev. Lett. **70**, 2154 (1993); S. Yücel, L. Menna, and E. Y. Andrei, Physica B **194-196**, 1223 (1994).
[11] (a) M. I. Dykman, T. Sharpee, and P. M. Platzman, Phys. Rev. Lett. **86**, 2408 (2001); (b) T. Sharpee, M. I. Dykman, and P. M. Platzman, Phys. Rev. B **64**, 245309 (2001).
[12] E. Abrahams, S. V. Kravchenko, and M. P. Sarachik, Rev. Mod. Phys. **73**, 251 (2001).
[13] (a) L. P. Kotova, A. M. Perelomov, and V. S. Popov, Zh. Eksp. Teor. Fiz. **54**, 1151 (1968) [Sov. Phys. JETP **27**, 616 (1968)]; (b) V. S. Popov, B. M. Karnakov, and V. D. Mur, Zh. Eksp. Teor. Fiz. **113**, 1579 (1998) [JETP **86**, 860 (1998)].
[14] A. O. Caldeira and A. J. Leggett, Ann. Phys. (N.Y.) **149**, 374 (1983).
[15] H. A. Fertig and B. I. Halperin, Phys. Rev. B **36**, 7969 (1987).
[16] P. Ao, Phys. Rev. Lett. **72**, 1898 (1994); Phys. Scr., T **T69**, 7 (1997).
[17] B. I. Shklovskii, Pis'ma Zh. Eksp. Teor. Fiz. **36**, 43 (1982) [JETP Lett. **36**, 51 (1982)].
[18] J. K. Jain and S. Kivelson, Phys. Rev. B **37**, 4111 (1988).
[19] B. Helffer and J. Sjöstrand, Ann. Scuola Norm. Sup. Pisa Cl. Sci. (4) **14**, 625 (1988).
[20] Qin Li and D. J. Thouless, Phys. Rev. B **40**, 9738 (1989).
[21] T. Martin and S. Feng, Phys. Rev. B **44**, 9084 (1991).
[22] J. Hajdu, M. E. Raikh, and T. V. Shahbazyan, Phys. Rev. B **50**, 17 625 (1994); M. E. Raikh and T. V. Shahbazyan, Phys. Rev. B **51**, 9682 (1995).
[23] S. Nakamura, Commun. Math. Phys. **200**, 25 (1999), and references therein.
[24] T. Barabash-Sharpee, M. I. Dykman, and P. M. Platzman, Phys. Rev. Lett. **84**, 2227 (2000).
[25] J. S. Langer, Ann. Phys. (N.Y.) **41**, 108 (1967).
[26] S. Coleman, Phys. Rev. D **15**, 2929 (1977); C. G. Callan and S. Coleman, *ibid.* **16**, 1762 (1977).
[27] A. Auerbach and S. Kivelson, Nucl. Phys. B **257**, 799 (1985).
[28] U. Eckern and A. Schmid, in *Quantum Tunnelling in Condensed Matter*, edited by Yu. Kagan and A. J. Leggett (Elsevier, New York, 1992), p. 145.
[29] Z. H. Huang, T. E. Feuchtwang, P. H. Cutler, and E. Kazes, Phys. Rev. A **41**, 32 (1990).
[30] J. Knoll and R. Schaeffer, Ann. Phys. (N.Y.) **97**, 307 (1976).
[31] M. V. Berry, Adv. Phys. **25**, 1 (1976); Proc. R. Soc. London, Ser. A **422**, 7 (1989); **427**, 265 (1990); J. Heading, *An Introduction to Phase-Integrals Methods* (Methuen, London, 1962).
[32] L. S. Schulman, *Techniques and Applications of Path Integration* (Wiley, New York, 1981).
[33] L. D. Landau and E. M. Lifshitz, *Quantum Mechanics: Nonrelativistic Theory* (Pergamon, New York, 1977).
[34] G. G. Stokes, Trans. Cambridge Philos. Soc. **10**, 106 (1857).
[35] M. V. Berry and K. E. Mount, Rep. Prog. Phys. **35**, 315 (1972).
[36] M. Ya. Azbel, Phys. Rev. Lett. **64**, 1553 (1990); M. Ya. Azbel and P. M. Platzman, *ibid.* **65**, 1376 (1990).
[37] R. P. Feynman and A. R. Hibbs, *Quantum Mechanics and Path Integrals* (McGraw-Hill, New York, 1965).
[38] C. M. Bender and S. Boettcher, Phys. Rev. Lett. **80**, 5243 (1998); C. M. Bender, S. Boettcher, and P. N. Meisinger, J. Math. Phys. **40**, 2201 (1999); C. M. Bender, M. Berry, P. N. Meisinger, van M Savage, and M. Simsek, J. Phys. A **34**, L31 (2001).
[39] M. I. Freidlin and A. D. Wentzel, *Random Perturbations in Dynamical Systems* (Springer, New York, 1984).
[40] R. Graham and T. Tél, Phys. Rev. Lett. **52**, 9 (1984); R. Graham and T. Tél, Phys. Rev. A **31**, 1109 (1985); R. Graham, in *Noise in Nonlinear Dynamical Systems*, edited by F. Moss and P. V. E. McClintock (Cambridge University Press, Cambridge, 1989), Vol. 1, p. 225.
[41] M. I. Dykman and M. A. Krivoglaz, Zh. Eksp. Teor. Fiz. **77**, 60 (1979) [Sov. Phys. JETP **50**, 30 (1979)]; M. I. Dykman, Phys. Rev. A **42**, 2020 (1990).
[42] M. I. Dykman, P. V. E. McClintock, V. N. Smelyanskiy, N. D. Stein, and N. G. Stocks, Phys. Rev. Lett. **68**, 2718 (1992); J. Hales, A. Zhukov, R. Roy, and M. I. Dykman, *ibid.* **85**, 78 (2000).
[43] (a) M. I. Dykman, M. M. Millonas, and V. N. Smelyanskiy, Phys. Lett. A **195**, 53 (1994); (b) M. I. Dykman, D. G. Luchinsky, P. V. E. McClintock, and V. N. Smelyanskiy, Phys. Rev. Lett. **77**, 5229 (1996).